EXTENDED PDF FORMAT
SPONSORED BY
usb
www.usbweb.com

Science

Directed Assembly of Block Copolymer Blends into Nonregular Device-Oriented Structures

Mark P. Stoykovich, *et al.*

Science **308**, 1442 (2005);
DOI: 10.1126/science.1111041

The following resources related to this article are available online at www.sciencemag.org (this information is current as of March 11, 2009):

Updated information and services, including high-resolution figures, can be found in the online version of this article at:
http://www.sciencemag.org/cgi/content/full/308/5727/1442

Supporting Online Material can be found at:
http://www.sciencemag.org/cgi/content/full/308/5727/1442/DC1

This article **cites 31 articles**, 4 of which can be accessed for free:
http://www.sciencemag.org/cgi/content/full/308/5727/1442#otherarticles

This article has been **cited by** 134 article(s) on the ISI Web of Science.

This article has been **cited by** 2 articles hosted by HighWire Press; see:
http://www.sciencemag.org/cgi/content/full/308/5727/1442#otherarticles

This article appears in the following **subject collections**:
Physics, Applied
http://www.sciencemag.org/cgi/collection/app_physics

Information about obtaining **reprints** of this article or about obtaining **permission to reproduce this article** in whole or in part can be found at:
http://www.sciencemag.org/about/permissions.dtl

Downloaded from www.sciencemag.org on March 11, 2009

Science (print ISSN 0036-8075; online ISSN 1095-9203) is published weekly, except the last week in December, by the American Association for the Advancement of Science, 1200 New York Avenue NW, Washington, DC 20005. Copyright 2005 by the American Association for the Advancement of Science; all rights reserved. The title *Science* is a registered trademark of AAAS.

also found good agreement with the published XRD data (*16*) (supporting online material text, figs. S2 and S3).

With 12 Al_s atoms in pyramids and 12 in tetrahedra and the nonhexagonal oxygen layer, the film is neither related to bulk corundum nor to bulk γ or κ alumina. This result shows that extrapolation from bulk materials to thin films, even if supplemented by chemical intuition, is often insufficient for the correct determination of complex structures. However, by applying the experiment and theory in a closely coupled manner, very complex structures—here, 92 atoms in the unit cell—can be solved unambiguously.

Finally, the structure of the ultrathin alumina film on NiAl(110) will provide a good starting point for understanding the structures of other oxide surfaces, especially those of Al_2O_3. For instance, the average Al-Al in-plane distance in the surface layer of the complex $\sqrt{31} \times \sqrt{31}$ surface reconstruction of corundum (0001) is 3.03 Å (*22*, *23*), exactly the same value as in the first Al layer of the ultrathin oxide on NiAl(110). This similarity suggests that the reduced corundum surface is built in a manner similar to the current structure, with exactly the same structural elements, resulting in an oxygen layer with square and hexagonal arrangements at the top and a distorted hexagonal Al layer slightly below.

References and Notes

1. H. Over *et al.*, *Science* **287**, 1474 (2000).
2. C. I. Carlisle *et al.*, *Phys. Rev. Lett.* **84**, 3899 (2000).
3. E. Lundgren *et al.*, *Phys. Rev. Lett.* **88**, 246103 (2002).
4. B. L. Hendriksen, J. W. Frenken, *Phys. Rev. Lett.* **89**, 046101 (2002).
5. N. Nilius, T. M. Wallis, W. Ho, *Phys. Rev. Lett.* **90**, 046808 (2003).
6. X. H. Qiu, G. V. Nazin, W. Ho, *Science* **299**, 542 (2003).
7. E. Lundgren *et al.*, *Phys. Rev. Lett.* **92**, 046101 (2004).
8. J. Gustafson *et al.*, *Phys. Rev. Lett.* **92**, 126102 (2004).
9. W. X. Li *et al.*, *Phys. Rev. Lett.* **93**, 146104 (2004).
10. R. M. Jaeger *et al.*, *Surf. Sci.* **259**, 235 (1991).
11. J. Libuda *et al.*, *Surf. Sci.* **318**, 61 (1994).
12. F. Winkelmann *et al.*, *Surf. Sci.* **307–309**, 1148 (1994).
13. M. Frank *et al.*, *Surf. Sci.* **492**, 270 (2001).
14. M. Kulawik, N. Nilius, H.-P. Rust, H.-J. Freund, *Phys. Rev. Lett.* **91**, 256101 (2003).
15. X. Torrelles *et al.*, *Surf. Sci.* **487**, 97 (2001).
16. A. Stierle *et al.*, *Science* **303**, 1652 (2004).
17. D. R. Jennison, A. Bogicevic, *Surf. Sci.* **464**, 108 (2000).
18. X.-G. Wang *et al.*, *Phys. Rev. Lett.* **84**, 3650 (2000).
19. Materials and methods are available as supporting material on *Science* Online.
20. STM simulations based on the Tersoff-Hamann approach [local density of states (LDOS) near the Fermi edge] show the O_s atoms as protrusions. At larger tip-surface distances, O_s atoms with Al_i atoms below become progressively brighter, because the tails of the NiAl states can more easily penetrate into the vacuum through the Al_i atoms. This is in agreement with the experimental observation that only these O_s atoms are visible for larger bias voltages, where the tip-surface distance is relatively large. Obtaining atomic resolution in the low-temperature STM at moderately high tunneling voltages as well as the appearance of the STM images in (*14*) indicate that the contrast observed in the low-temperature images is not due to simple LDOS but rather due to an adsorbate at the tip interacting with the surface Al atoms, similar to the process discussed for chemical contrast on alloys (*24*). This type of image was not observed at room temperature, indicating that the adsorbate is not stable at the tip at room temperature.
21. At typical growth conditions, the chemical potentials μ_{Al} and μ_O can be estimated to be roughly 1 eV smaller than the formation energy of bulk face-centered cubic Al and O_2, respectively (*25*, *26*).
22. G. Renaud, B. Villette, I. Vilfan, A. Bourret, *Phys. Rev. Lett.* **73**, 1825 (1994).
23. C. Barth, M. Reichling, *Nature* **414**, 54 (2001).
24. M. Schmid, H. Stadler, P. Varga, *Phys. Rev. Lett.* **70**, 1441 (1993).
25. M. Hagen, M. W. Finnis, *Philos. Mag. A* **77**, 447 (1998).
26. K. Reuter, M. Scheffler, *Phys. Rev. B* **65**, 035406 (2002).

27. We thank H.-J. Freund for helpful discussions and for lending an NiAl single crystal to us. This work was supported by the Austrian Fonds zur Förderung der wissenschaftlichen Forschung.

Supporting Online Material
www.sciencemag.org/cgi/content/full/308/5727/1440/DC1
Materials and Methods
SOM Text
Figs. S1 to S3
Table S1

22 November 2004; accepted 7 April 2005
10.1126/science.1107783

Directed Assembly of Block Copolymer Blends into Nonregular Device-Oriented Structures

Mark P. Stoykovich,[1] Marcus Müller,[2] Sang Ouk Kim,[3] Harun H. Solak,[4] Erik W. Edwards,[1] Juan J. de Pablo,[1] Paul F. Nealey[1]†

Self-assembly is an effective strategy for the creation of periodic structures at the nanoscale. However, because microelectronic devices use free-form design principles, the insertion point of self-assembling materials into existing nanomanufacturing processes is unclear. We directed ternary blends of diblock copolymers and homopolymers that naturally form periodic arrays to assemble into nonregular device-oriented structures on chemically nanopatterned substrates. Redistribution of homopolymer facilitates the defect-free assembly in locations where the domain dimensions deviate substantially from those formed in the bulk. The ability to pattern nonregular structures using self-assembling materials creates new opportunities for nanoscale manufacturing.

One of the challenges in nanofabrication is the integration of self-assembling materials into existing manufacturing strategies to achieve molecular-level process control and the ability to produce useful architectures. Previous reports of block copolymer lithography described an inexpensive, parallel, and scalable technique for patterning dense periodic arrays of nanostructures (*1*) that are suited for a number of applications such as nanowires (*2*, *3*), quantum dots (*1*, *4*), magnetic storage media (*5*), flash memory devices (*6*), photonic crystals (*7*), and silicon capacitors (*8*). Diblock copolymers consist of two chemically connected polymer chains. Because of their different properties, the chain segments tend to spontaneously form ordered nanostructures, including spheres, cylinders, and lamellae, whose shape and dimensions depend on the molecular weight and composition of the polymer (*9*). Block copolymer lithography refers to the use of these ordered structures in the form of thin films as patterning templates. Varying degrees of long-range order and substrate registration of the periodic arrays are achieved by using strategies such as electric fields (*2*, *10*), chemically (*11–13*) and topographically (*14–16*) patterned substrates, and shear (*17*). We demonstrate that, by directing the assembly of blends of block copolymers and homopolymers on chemically nanopatterned substrates, it is possible to pattern nonregular-shaped structures aided by a nonuniform distribution of homopolymers across the patterns. The technological implication of this approach is that the fine control of structure dimensions afforded by self-assembling block copolymer materials may be harnessed for applications such as the production of nanoelectronic devices that require patterns more complex than simple periodic arrays.

Current commercial lithographic processes can generate patterns with perfection over macroscopic areas and with dimensional control of features, registration, and overlay within exacting tolerances and margins. In the past decade, considerable resources have been

[1]Department of Chemical and Biological Engineering and Center for Nanotechnology, University of Wisconsin (UW), Madison, WI 53706, USA. [2]Department of Physics, University of Wisconsin, Madison, WI 53706, USA. [3]Department of Materials Science and Engineering, Korea Advanced Institute of Science and Technology, Daejeon 305-701, Republic of Korea. [4]Laboratory for Micro- and Nanotechnology, Paul Scherrer Institute, CH-5232 Villigen PSI, Switzerland.

†To whom correspondence should be addressed. E-mail: nealey@engr.wisc.edu

Downloaded from www.sciencemag.org on March 11, 2009

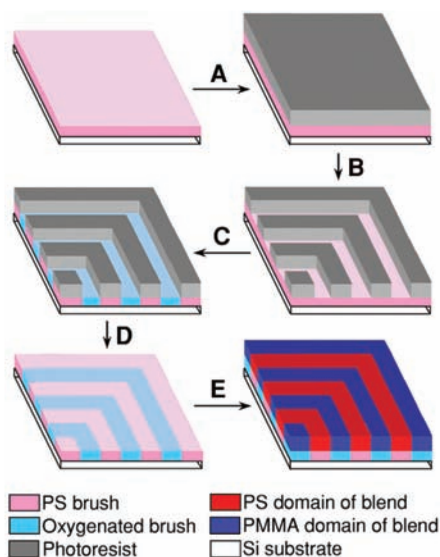

Fig. 1. Schematic of the process used to fabricate chemically nanopatterned surfaces that direct the self-assembly of ternary blends in linear and bend geometries. (**A**) A photoresist was spin-coated on a PS brush that was grafted to a Si substrate and (**B**) patterned by using advanced lithography to produce line and space features of period L_S. (**C**) Oxygen plasma etching was used to chemically modify the exposed regions of the PS brush and to convert the topographic photoresist pattern into a chemical surface pattern. (**D**) The photoresist was removed by solvent treatment, and (**E**) a ternary block copolymer–homopolymer blend was coated and annealed on the chemical surface pattern.

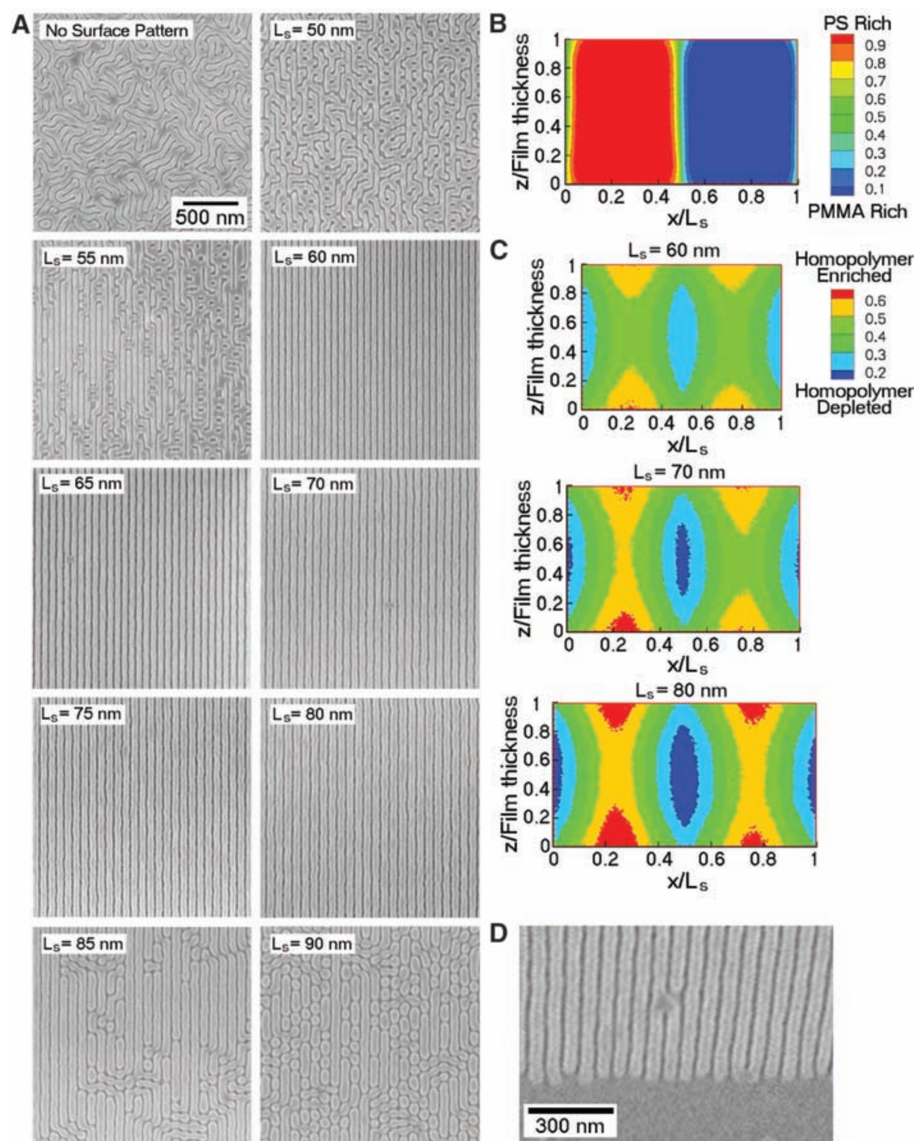

Fig. 2. Behavior of ternary blends on chemical surface patterns with linear geometries. (**A**) Top-down SEM images of the ternary PS-b-PMMA/PS/PMMA blend (L_B = 70 nm) on an unpatterned neutral surface of PS-r-PMMA and on chemically striped PS surfaces. The chemical surface patterns have a period, L_S, ranging from 50 to 90 nm. Each micrograph depicts a 2 μm by 2 μm area. The bright and dark regions correspond to the PS and PMMA domains, respectively, and the dimensions of the PS domains appear artificially large because of the SEM imaging. (**B**) Contour plot of the relative composition of PS segments in a single lamellar period ($L_S = L_B$ = 70 nm) as obtained from two-dimensional SCMF simulations. The PS- and PMMA-rich domains are shown in red and blue, respectively. (**C**) Contour plots of the relative concentration of both homopolymers, PS and PMMA, from SCMF simulations of defect-free morphologies of the ternary blend on linear surface patterns with L_S of 60, 70, and 80 nm. The centers of the lamellar domains are enriched in homopolymers (shown in red), whereas the domain interfaces are depleted of homopolymers (shown in blue). The contour plots of (B) and (C) are displayed as a cross section of the thin film, where *x* is the direction normal to the lamellae and *z* is the direction normal to the substrate (z/film thickness = 0) and free surface (z/film thickness = 1). The data have been averaged in the direction parallel to the lamellae. (**D**) Top-down SEM image of the ends of line structures. The perpendicular lamellar domains (top portion) terminate at a boundary with lamellae oriented parallel to the substrate (bottom portion). The end of the chemical surface pattern has a period of L_S = 60 nm, whereas at the top of the image $L_S \approx 63$ nm.

allocated to the development of exposure tools capable of resolving nanoscale patterns (< 30 nm) with the required registration and overlay capabilities, but relatively modest investments have been made in the development of suitable imaging materials at this length scale (*18*). Currently chemically amplified photoresists are used in manufacturing processes to pattern features with dimensions as small as 50 to 70 nm but may not be extendable as feature dimensions shrink to 30 nm and below. Other types of photoresists and electron beam lithography have been used to fabricate proof-of-principle devices with features below 10 nm (*19*, *20*). Although these demonstrations provide motivation for continuing to push the limits of nanomanufacturing, the materials and processes themselves are not amenable for production purposes in their present form (*20*). Self-assembling materials used in conjunction with the most advanced exposure tools may enable extension of current manufacturing practices to dimensions of 10 nm and less. Recently we demonstrated that the domains of block copolymer films could be directed to assemble into defect-free periodic patterns over arbitrarily large areas in registry with lithographically defined chemical surface patterns (*11*, *21*) and with nanometer precision over the lateral dimensions of the domains (*22*). We now extend the capabilities of block copolymer lithography to include patterns of line segments and nested arrays of lines with sharp bends by using ternary blends of diblock copolymers and homopolymers.

The schematic in Fig. 1 illustrates the process used to fabricate chemically nanopatterned surfaces that subsequently direct the assembly of films of ternary block copolymer-homopolymer blends (*11*, *22*). Hydroxy-terminated polystyrene (PS) was

Downloaded from www.sciencemag.org on March 11, 2009

grafted to a silicon substrate, resulting in a PS brush layer (*22–24*). The PS brush was then coated with a thin film of photoresist. Advanced lithography was used to pattern the photoresist with arrays of roughly equal lines and spaces having periods between 50 and 90 nm and bends with angles from 45° to 135°. Patterning was performed by electron beam lithography for all features with periods ≥ 60 nm and by extreme ultraviolet interference lithography (*25*) for features with periods < 60 nm (*24*). The sample was then subjected to an oxygen plasma. The surface was chemically modified and rendered strongly hydrophilic or polar only in areas where the photoresist did not cover the PS brush (*24*). The remaining photoresist was removed by solvent rinses, leaving behind the chemically nanopatterned surface. A ~43-nm film of a ternary block copolymer–homopolymer blend was subsequently spin-coated and annealed on the patterned surface at 193°C for 7 days (*24*). These block copolymer films have an adequate thickness to act as templates for patterning through selective etching or deposition processes (*1*, *3*, *5*, *8*) and are sufficiently thin for the surface interactions to stabilize the perpendicular morphology (*21*). The ternary blend consisted of 60 weight % (wt. %) symmetric polystyrene-block-poly(methyl methacrylate) (PS-b-PMMA, 104 kg mol^{-1}, bulk lamellar period of L_O = 49 nm), 20 wt. % polystyrene homopolymer (PS, 40 kg mol^{-1}), and 20 wt. % poly(methyl methacrylate) homopolymer (PMMA, 41 kg mol^{-1}). On homogeneous neutral wetting surfaces, the blend formed a lamellar phase with a period, L_B, of 70 nm (Fig. 2A) (*26*). The PS domain of the ternary blend preferentially wet the unmodified PS brush, and the PMMA domain preferentially wet the regions of the brush that were chemically modified by the oxygen plasma. Scanning electron microscopy (SEM) was used to image the domain structure of the block copolymer blend after annealing.

Top-down SEM images of the domain structure of the ternary blend with L_B = 70 nm on surfaces with striped chemical nanopatterns of period L_S between 50 to 90 nm are shown in Fig. 2A. Lamellae were perfectly ordered and registered on surfaces having L_S ranging from 60 to 80 nm. For L_S < 60 nm, compression of the lamellar domains led to the formation of bridges between domains that were predominately oriented perpendicular to the surface pattern. For L_S > 80 nm, the lamellar structures appeared to be pinched off into small, circular domains of PS or PMMA. For L_S = 85 nm, the circular domains, although remaining centered and registered with the underlying chemical pattern, had an increased propensity to merge with neighboring domains on adjacent surface stripes. For L_S = 90 nm there were few aligned lamellae and more circular domains. These defect structures in the blends are distinctly different than the dislocations and disclinations observed at incommensurate values of L_S and L_O for pure block copolymers (*11*, *22*). The range of L_S over which perfect directed assembly was achieved with the blends, however, is consistent with previous results using pure block copolymers (*22*).

Single chain in mean field (SCMF) simulations, a particle-based self-consistent field method, were performed to calculate the molecular-level distribution of homopolymers within the lamellar domains as a function of L_S (*24*, *27*). Self-consistent field techniques (*28*) have been shown to accurately describe the self-assembly of block copolymers in the bulk (*29*) and under confinement (*30*). The calculations use values of χN, where χ is the Flory-Huggins interaction parameter taken from the literature and N is the degree of polymerization, and the length scale as determined from the lamellar period of the blend, L_B, on unpatterned surfaces. Figure 2B presents a contour plot of the composition of perfectly aligned ternary blend domains on a chemically striped surface ($L_S = L_B$ = 70 nm). The interfaces between the PS and PMMA domains are found to be sharp for 60 nm ≤ L_S ≤ 80 nm. However, the distribution of homopolymer in the domains varies with L_S (Fig. 2C). In defect-free lamellae with $L_S \geq L_B$, the homopolymers are concentrated primarily at the center of the domains, and an absence of homopolymer is observed near the domain interfaces. The degree of homopolymer segregation to the center of the domains increases with increasing period mismatch, L_S/L_B. Surface patterns with $L_S < L_B$ induce a spatially more uniform homopolymer distribution within the domains. Moreover, the homopolymer within the lamellar domains exhibits a tendency to segregate toward the substrate interface and the free surface because of its lower molecular weight.

A representative image of the ends of line structures is shown in Fig. 2D. Here, perpendicular lamellar domains on underlying chemical patterns terminate at a boundary with lamellae oriented parallel to the substrate assembled on a chemically homogeneous (PS brush) region of the surface. These structures form templates for patterning line segments that terminate at precise locations.

Nested arrays of lines with sharp bends represent model test features for the type of patterns currently used in the free-form logic devices of microprocessors and integrated circuits. Figure 3 shows the directed assembly of nested arrays of lines with different bend geometries. Periods in the linear sections of the chemical surface pattern, L_S, ranged from 65 to 80 nm such that $L_S \sim L_B$ = 70 nm. The linear portions of the blend lamellae were defect-free for all of the examined periods. In addition, the ternary blend formed defect-free lamellae on surface patterns of 45°, 90°, and 135° bends. Perfect assembly was observed on the 45° bends for all examined L_S, but perfect structures were formed on the 90° and 135° bends only for patterns of L_S ≤ 70 nm and L_S ≤ 65 nm, respectively.

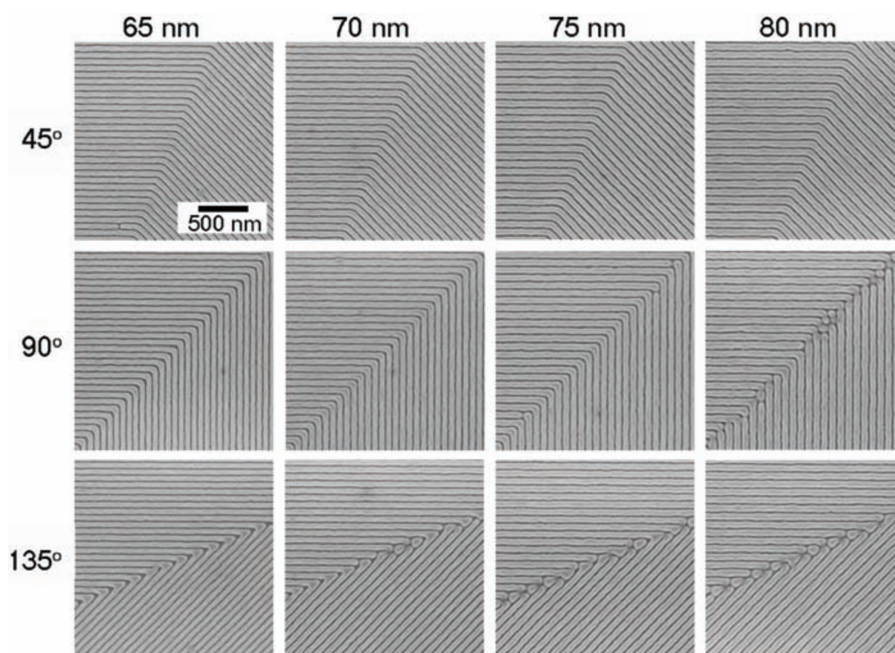

Fig. 3. Top-down SEM images of angled lamellae in a ternary PS-b-PMMA/PS/PMMA blend (L_B = 70 nm). The chemical surface patterns are fabricated with L_S values of 65, 70, 75, and 80 nm, and the lamellar domains of the block copolymer blend are self-assembled and registered around 45°, 90°, and 135° bends. Perfect long-range order was achieved in the linear portions for all L_S, whereas defects arose at the corners of the 90° bends for L_S ≥ 75 nm and the 135° bends for L_S ≥ 70 nm. The micrographs each depict a 2 μm by 2 μm area.

Downloaded from www.sciencemag.org on March 11, 2009

The differences in domain structure and the formation of defects at the corners of the 45°, 90°, and 135° bends (Fig. 3) depend on the bend angle, θ, and the corner-to-corner lamellar period, L_C (Fig. 4A). Lamellae in the corners of the L_S = 80 nm and 90° bends began to connect with adjacent lamellar domains. For $L_S \geq 70$ nm and 135° bends, the corners were primarily occupied by isolated, round PS domains. These types of defects are similar to those observed on linear chemical surface patterns with $L_S > 80$ nm (Fig. 2A). To a first approximation, one expects the defect-free ordering of lamellae if the corner-to-corner period, $L_C = L_S/\cos(\theta/2)$, is smaller than the largest period [80 nm (compare with Fig. 2A)] of chemical surface stripes on which perfect ordering was observed. For L_S = 70 nm and θ = 90°, however, L_C was 99 nm (≫ 80 nm), but corner defects were not observed experimentally. The underestimation of the stability of defect-free bends by this simple geometric argument suggests that localized redistribution of homopolymer must occur at the bend corners.

SCMF simulations of the directed assembly of ternary blends on surfaces chemically patterned with bend geometries ($L_S = L_B$ = 70 nm) confirm the presence of homopolymer-rich material in the bend corners. Similar to the experimental results, defect-free ordering is observed in the SCMF results for θ values of 45° and 90° (Fig. 4B), and defects arise for the largest bend angle, θ = 135°. The SCMF results in Fig. 4C reveal that the local concentration of homopolymers is greatest in the middle of the corners. For the plots of homopolymer–block copolymer concentration as a function of position (Fig. 4C), the periodicity of the apparent pattern is twice that of the pattern of PS and PMMA domains (Fig. 4B), indicative of alternating regions rich in PS homopolymer and in PMMA homopolymer (both shown in red) separated by block copolymer–rich interfaces (shown in blue). This local redistribution of homopolymer is more pronounced on the 90° bends than on the 45° bends. Figure 4D shows that the concentration profile of homopolymer decays along a line moving away from the corners. The length scale over which homopolymers are recruited to the corners is large, and there is a noticeable depletion of the homopolymers in the linear portions of the domains away from the corners. Although the 45° bends have a nearly bulk homopolymer concentration of ~40 volume % (vol. %) in the linear portions, the 90° bends display a uniformly reduced homopolymer concentration of ~39 vol. % throughout the examined linear region.

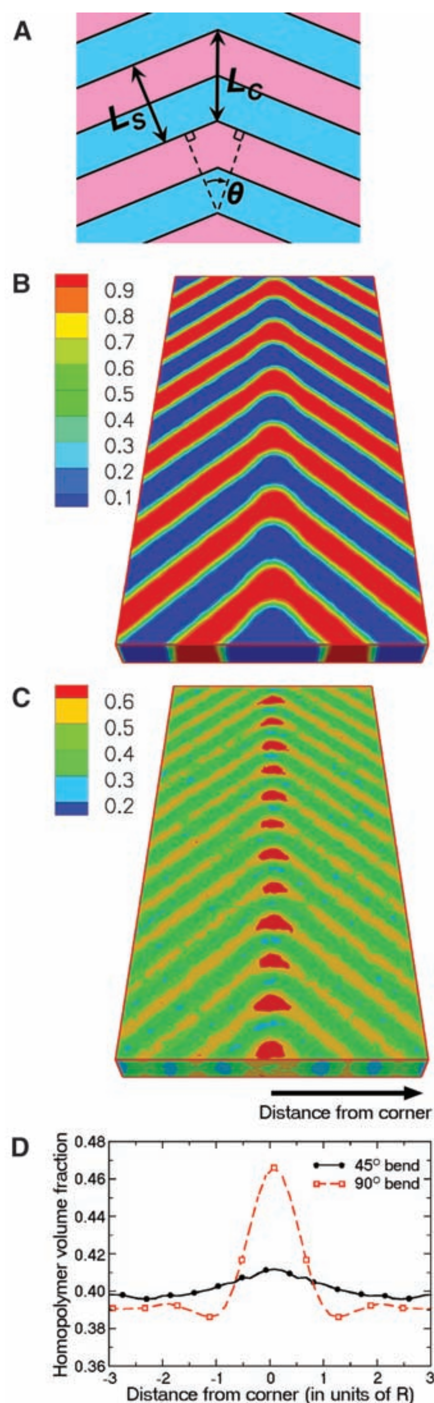

Fig. 4. (**A**) Schematic of the increased lamellar period at the corners of the bends. The linear structures have a lamellar period of L_S, whereas the corner-to-corner lamellar period is L_C such that $L_C > L_S$. Three-dimensional contour plots of (**B**) the PS concentration and (**C**) the total homopolymer concentration obtained from SCMF simulations for $L_S = L_B$ = 70 nm show the segregation of homopolymers to the 90° bend corners (contour levels identical to those in Fig. 2). In (B), the red and blue areas represent PS- and PMMA-rich domains, respectively. In (C), the periodic red areas are enriched alternatively in PS and PMMA homopolymers, whereas the blue stripes represent the domain interfaces that are depleted of homopolymers. The images display the simulated system of area 9.63R by 19.26R (0.3 μm by 0.6 μm), where $R \approx 31$ nm is the magnitude of the diblock copolymer's end-to-end vector. (**D**) Averaged total homopolymer concentration as a function of the distance from the line of corners for 45° and 90° bends. Upon increasing the bend angle, we observed an increased segregation of the homopolymers to the corners. The enrichment zone is of comparable width to the lamellar spacing and is followed by a depletion zone further away from the corners.

Nested arrays of bent lines are used routinely to benchmark photoresists, but these structures are also reminiscent of metastable defects formed at tilt grain boundaries in the bulk (*31*–*33*). The presence of homopolymer in block copolymer–homopolymer blends mitigates the free energy cost and changes the type of defect observed as a function of tilt angle (*32*, *33*). In contrast to these metastable defects at grain boundaries, the chevron-like structures formed on chemically patterned surfaces are in thermodynamic equilibrium, and structures analogous to omega and T-junction grain boundary defects are not observed at any bend angle. This analysis highlights the relatively large contribution of the polymer-substrate interfacial energy to the overall free energy of sufficiently thin films, which enables the directed assembly of block copolymer domains into structures that do not exist in the bulk [Supporting Online Material (SOM) Text].

The extension of block copolymer lithography to pattern features more complex than simple periodic arrays creates opportunities for widespread use of these nontraditional imaging materials in nanofabrication. Because pattern formation was facilitated through enriched or depleted concentrations of homopolymer depending on the local dimensions of the structures, it may be possible to create relatively high densities of many different types of nonregular shaped structures used in device manufacturing by optimizing blend compositions, polymer chemistry, and interfacial interactions. Our approach retains the essential attributes of current lithographic materials and processes, including pattern perfection and registration, but may be scaled to dimensions of 10 nm or below with precise control over feature size and shape.

References and Notes

1. M. Park, C. Harrison, P. M. Chaikin, R. A. Register, D. H. Adamson, *Science* **276**, 1401 (1997).
2. T. Thurn-Albrecht *et al.*, *Science* **290**, 2126 (2000).
3. W. A. Lopes, H. M. Jaeger, *Nature* **414**, 735 (2001).
4. R. R. Li *et al.*, *Appl. Phys. Lett.* **76**, 1689 (2000).
5. J. Y. Cheng *et al.*, *Adv. Mater.* **13**, 1174 (2001).
6. K. W. Guarini *et al.*, in *International Electron Devices Meeting Technical Digest* (IEEE, Piscataway, NJ, 2003), pp. 541–544.
7. A. Urbas *et al.*, *Adv. Mater.* **12**, 812 (2000).
8. C. T. Black *et al.*, *Appl. Phys. Lett.* **79**, 409 (2001).
9. F. S. Bates, G. H. Fredrickson, *Annu. Rev. Phys. Chem.* **41**, 525 (1990).
10. T. L. Morkved *et al.*, *Science* **273**, 931 (1996).
11. S. O. Kim *et al.*, *Nature* **424**, 411 (2003).
12. L. Rockford *et al.*, *Phys. Rev. Lett.* **82**, 2602 (1999).
13. X. M. Yang, R. D. Peters, P. F. Nealey, H. H. Solak, F. Cerrina, *Macromolecules* **33**, 9575 (2000).
14. R. A. Segalman, H. Yokoyama, E. J. Kramer, *Adv. Mater.* **13**, 1152 (2001).

Downloaded from www.sciencemag.org on March 11, 2009

15. J. Y. Cheng, A. M. Mayes, C. A. Ross, *Nat. Mater.* **3**, 823 (2004).
16. D. Sundrani, S. B. Darling, S. J. Sibener, *Nano. Lett.* **4**, 273 (2004).
17. D. E. Angelescu *et al.*, *Adv. Mater.* **16**, 1736 (2004).
18. D. J. C. Herr, in *Future Fab International*, B. Dustrud, Ed. (Montgomery Research Incorporated, San Francisco, CA, 2005), issue 18, chap. 5.
19. J. Fujita, Y. Ohnishi, Y. Ochiai, S. Matsui, *Appl. Phys. Lett.* **68**, 1297 (1996).
20. K. E. Gonsalves, L. Merhari, H. Wu, Y. Hu, *Adv. Mater.* **13**, 703 (2001).
21. Q. Wang, S. K. Nath, P. F. Nealey, J. J. de Pablo, *J. Chem. Phys.* **112**, 9996 (2000).
22. E. W. Edwards, M. F. Montague, H. H. Solak, C. J. Hawker, P. F. Nealey, *Adv. Mater.* **16**, 1315 (2004).
23. P. Mansky, Y. Liu, E. Huang, T. P. Russell, C. Hawker, *Science* **275**, 1458 (1997).
24. Additional materials and methods information is available on *Science* Online.
25. H. H. Solak *et al.*, *Microelectron. Eng.* **67–68**, 56 (2003).
26. The lamellar spacing of the ternary block copolymer–homopolymer blends can be controlled over a wide range of values by changing the volume fraction of homopolymer. Little is known about their behavior in the form of thin films, but previous studies of phase diagrams and morphology in the bulk (*34*, *35*) provide useful insights.
27. M. Müller, G. D. Smith, *J. Polym. Sci. B* **43**, 934 (2005).
28. G. H. Fredrickson, V. Ganesan, F. Drolet, *Macromolecules* **35**, 16 (2002).
29. M. W. Matsen, F. S. Bates, *Macromolecules* **29**, 1091 (1996).
30. A. Knoll *et al.*, *Nat. Mater.* **3**, 886 (2004).
31. S. P. Gido, E. L. Thomas, *Macromolecules* **27**, 6137 (1994).
32. E. Burgaz, S. P. Gido, *Macromolecules* **33**, 8739 (2000).
33. D. Duque, K. Katsov, M. Schick, *J. Chem. Phys.* **117**, 10315 (2002).
34. F. S. Bates *et al.*, *Phys. Rev. Lett.* **79**, 849 (1997).
35. D. Broseta, G. H. Fredrickson, *J. Chem. Phys.* **93**, 2927 (1990).

36. This research was supported by the Semiconductor Research Corporation (SRC) (2002-MJ-985), NSF through the Nanoscale Science and Engineering Center (DMR-0425880), and the Camille Dreyfus Teacher-Scholar Award. This work made use of the facilities and staff at the UW Center for Nanotechnology, the Synchrotron Radiation Center at UW Madison (NSF DMR-0084402), and the Swiss Light Source at the Paul Scherrer Institute. The authors thank the John von Neumann-Institute for Computing, Jülich, Germany, for central processing unit time on the IBM p690-cluster. M.P.S. acknowledges a research fellowship from the SRC Graduate Fellowship Program.

Supporting Online Material
www.sciencemag.org/cgi/content/full/308/5727/1442/DC1
Materials and Methods
SOM Text
Fig. S1

14 February 2005; accepted 18 April 2005
10.1126/science.1111041

Production of Liquid Alkanes by Aqueous-Phase Processing of Biomass-Derived Carbohydrates

George W. Huber, Juben N. Chheda, Christopher J. Barrett, James A. Dumesic*

Liquid alkanes with the number of carbon atoms ranging from C_7 to C_{15} were selectively produced from biomass-derived carbohydrates by acid-catalyzed dehydration, which was followed by aldol condensation over solid base catalysts to form large organic compounds. These molecules were then converted into alkanes by dehydration/hydrogenation over bifunctional catalysts that contained acid and metal sites in a four-phase reactor, in which the aqueous organic reactant becomes more hydrophobic and a hexadecane alkane stream removes hydrophobic species from the catalyst before they go on further to form coke. These liquid alkanes are of the appropriate molecular weight to be used as transportation fuel components, and they contain 90% of the energy of the carbohydrate and H_2 feeds.

The production of liquid fuels from renewable biomass resources is particularly attractive because gasoline- and diesel-powered hybrid electric vehicles are being developed that have overall energy efficiencies comparable to those of vehicles powered by fuel cells based on current technologies (*1*). Approximately 75% of the dry weight of herbaceous and woody biomass is composed of carbohydrates (*2*). Several processes currently exist to convert carbohydrates to liquid fuels, including the formation of bio-oils by liquefaction or pyrolysis of biomass (*3*), the production of alkanes or methanol by Fischer-Tropsch synthesis from biomass-derived $CO:H_2$ gas mixtures (*2*), and the conversion of sugars and methanol to aromatic hydrocarbons over zeolite catalysts (*4*, *5*).

However, the conversion of glucose to ethanol is the most widely practiced process (*6*) for producing liquid fuels from biomass, with an overall energy efficiency from corn (the heating value of ethanol divided by the energy required to produce ethanol from corn) equal to about 1.1 without coproduct energy credits (*7*). Approximately 67% of the energy required for ethanol production is consumed in the fermentation/distillation process, of which over half is used to distill ethanol from water (*7*, *8*).

In comparison, the production of alkanes from aqueous carbohydrate solutions would involve the spontaneous separation of the alkanes from water. Accordingly, we estimate that the overall energy efficiency for alkane production from corn would be increased to approximately 2.2, if we assume that this process eliminates the energy-intensive distillation step but still requires all of the remaining energy inputs needed for the production of ethanol from corn (*9*).

We have recently shown how an aqueous solution of sorbitol (the sugar-alcohol of glucose) can be converted to hexane (Eq. 1) with a catalyst containing both acid (e.g., SiO_2-Al_2O_3) and metal (e.g., Pt or Pd) sites to catalyze dehydration and hydrogenation reactions, respectively (*10*). Hydrogen for this reaction can be produced from the aqueous-phase reforming of sorbitol (Eq. 2) in the same reactor or in a separate reactor with a non-precious metal catalyst (*11*). The net reaction (Eq. 3) is an exothermic process in which approximately 1.5 mol of sorbitol produce 1 mol of hexane.

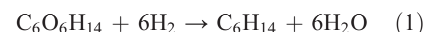

$$C_6O_6H_{14} + 6H_2 \rightarrow C_6H_{14} + 6H_2O \quad (1)$$

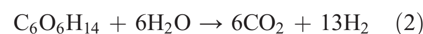

$$C_6O_6H_{14} + 6H_2O \rightarrow 6CO_2 + 13H_2 \quad (2)$$

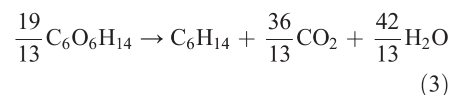

$$\frac{19}{13}C_6O_6H_{14} \rightarrow C_6H_{14} + \frac{36}{13}CO_2 + \frac{42}{13}H_2O \quad (3)$$

Alkanes produced in the aqueous-phase dehydration/hydrogenation (APD/H) of carbohydrates would provide a renewable source of transportation fuel to complement the rapidly growing production of biodiesel from vegetable oils and animal fats (*12*). Unfortunately, the high volatility of hexane makes this compound of low value as a fuel additive (*13*). Thus, the production of high-quality liquid fuels from carbohydrates requires the formation of larger alkanes, and this production can be accomplished by first linking carbohydrate-derived moieties through the formation of C-C bonds before APD/H processing. Here we present a catalytic process for the conversion of biomass-derived carbohydrates to liquid alkanes in the higher mass ranges (from C_7 to C_{15}) that can be used as sulfur-free fuel components. We note that C-O-C linkages (as found in disaccharides) are broken under APD/H reaction conditions. The formation of C-C bonds between carbohydrate-derived moieties can be carried out by a variety of chemical routes, and we have chosen a dehydration step (acid-catalyzed) followed by an aldol-condensation (base-catalyzed) step (Fig. 1).

Our current APD/H process cannot be used to produce alkanes from large water-soluble organic compounds because extensive amounts of coke form on the catalyst surface (between

Department of Chemical and Biological Engineering, University of Wisconsin at Madison, Madison, WI 53706, USA.

*To whom correspondence should be addressed. E-mail: dumesic@engr.wisc.edu

Downloaded from www.sciencemag.org on March 11, 2009